Konrad-Zuse-Zentrum
für Informationstechnik Berlin

Takustraße 7
D-14195 Berlin-Dahlem
Germany

R. EHRIG, O. OFENLOCH, K. SCHABER, P. DEUFLHARD

Modelling and Simulation of Aerosol Formation by Heterogeneous Nucleation in Gas–Liquid Contact Devices

ZIB-Report 01-15 (Juli 2001)

Modelling and Simulation of Aerosol Formation by Heterogeneous Nucleation in Gas–Liquid Contact Devices

R. Ehrig[1], O. Ofenloch[2], K. Schaber[2], P. Deuflhard[1]

4th July 2001

Abstract

This paper describes a new simulation tool for the prediction of aerosol formation and behavior in gas–liquid contact devices such as absorbers, scrubbers, quench coolers, and condensers as well as multistage gas cleaning processes, respectively.

Aerosol formation can impact severely the separation efficiency of gas cleaning processes. Aerosol or fog formation can arise by spontaneous condensation or desublimation in supersaturated gas phases.

The rigorous description of the mass and energy transfer between the gas phase, the liquid phase, and the growing aerosol droplets leads to a system of partial differential and algebraic equations. For the solution of these systems we have developed the plant simulation tool **AerCoDe**. This program bases upon the linearly–implicit Euler discretisation, which in combination with extrapolation permits an adaptive step size and order control.

Typical simulation results of a multistage industrial flue gas scrubbing process are presented. It is shown, that experimental data can be confirmed if the number concentration of condensation nuclei as an input parameter is roughly known.

Keywords: aerosols, heterogeneous nucleation, two–phase flow, balance equations, differential–algebraic equations, extrapolation methods

Mathematical Subject Classification: 65L80, 65N40, 76T10, 80A20

[1]Konrad–Zuse–Zentrum für Informationstechnik Berlin
[2]Institut für Technische Thermodynamik und Kältetechnik, Universität Karlsruhe

Contents

1 Introduction

Since several years, the phenomenon of undesired aerosol formation, or fog formation, respectively, in industrial gas cleaning or separation processes has been identified as a reason for various severe problems, like unacceptably high pollutant concentrations in exhaust gases [1, 2, 3] or contamination of products in downstream process steps.
In gas–liquid contact devices like absorbers, scrubbers, quench coolers, or condensers, aerosols can be formed by spontaneous condensation or desublimation in supersaturated gas–vapour mixtures.
Supersaturation is a necessary precondition of spontaneous phase transitions and aerosol formation. The degree of saturation $\mathbf{S}$ in a multicomponent mixture of a inert carrier gas and K condensable (vapour) components can be defined by

$$\mathbf{S} = \frac{p(T, y_1^{\mathrm{G}}, \ldots, y_K^{\mathrm{G}})}{p_s(T, y_1^{\mathrm{G}}, \ldots, y_K^{\mathrm{G}})} \quad , \tag{1}$$

where p is the actual total pressure of all vapour components i ($i = 1, \ldots, K+1$, component $K+1$ being the inert gas) and p_s the total equilibrium pressure at the dew point of the vapour mixture.
The total pressure p or p_s, respectively, can be calculated as the sum of the individual partial pressures of all condensable components according to Dalton.
Excluding chemical reactions in the gas phase, supersaturation ($\mathbf{S} > 1$) in a gas–liquid contact device can arise if the dew line is crossed by the process trajectory (or process path) which describes the change of state of the gas phase due to simultaneous heat and mass transfer between both phases. The saturation $\mathbf{S}$ has to exceed a critical barrier before nucleation and consequently aerosol formation can take place. Two nucleation mechanisms can be distinguished. Homogeneous nucleation occurs if critical molecule clusters, so called nuclei, are formed only by molecules of condensable components. This mechanism requires a high degree of critical saturation $\mathbf{S}_{\mathrm{crit}}$.
If gas borne fine particles are present, aerosol formation can be initiated by heterogeneous nucleation, which requires only a very small critical supersaturation close to unity [4, 5]. Heterogeneous nucleation is the dominant mechanism of aerosol formation in industrial gas cleaning processes, because one can find a high number of ultra fine wettable particles in many process gases, especially in flue gases [6]. After nucleation the aerosol droplets grow by condensation until the supersaturation of the gas phase disappears.
A detailed survey on the basic principles of aerosol formation in absorption, scrubbing and condensation processes and the research results in this field is given by Schaber [1, 7]. There, it has been shown that aerosols can be formed in absorption processes if high–strength inorganic acid gases like SO_3 (H_2SO_4), HCl, HBr or HNO_3 are absorbed in aqueous solutions.

If SO_3 or H_2SO_4, respectively, is absorbed in aqueous solutions, homogeneous nucleation is possible, because high degrees of saturation may occur. For all the other acid gases homogeneous, nucleation on absorption can be excluded due to relatively low supersaturation at typical industrial process operation conditions. That means, for example, HCl–aerosols are only formed, if a sufficient concentration of wettable fine particles is present.
In condensation processes, heterogeneous nucleation as well as homogeneous nucleation can take place. Especially, if saturated gas mixtures are cooled at high temperature differences between gas and cooling liquid, high supersaturation and consequently homogeneous nucleation may occur [8, 9, 10, 1].
In various investigations, characteristic aerosol parameters in absorption and condensation processes have been measured with optical in situ methods [7, 6, 11]. These measurements yield typical aerosol droplet sizes between 0.5 and 3 μm and number concentrations of droplets mainly between 10^5 and $5 \cdot 10^6$ cm^{-3}. This corresponds to typical number concentrations of wettable condensation nuclei in industrial waste gases. The upper limit of condensation nuclei is caused by Brownian coagulation of fine particles. A higher number concentration of particles is reduced quickly within a gas residence time lower than ten seconds.
In this paper the new plant simulation tool **AerCoDe** (Aerosol Formation in Contact Devices) based on heterogeneous nucleation is presented.
A key feature of this code is that the material and energy balances as well as the transport equations between both, the gas and liquid phase of a contact device on one hand, as well as the growing aerosol droplets and the supersaturated gas phase on the other hand are solved simultaneously. Thus it is possible to calculate the actual saturation of the gas and to predict the growth of aerosol droplets along the interfacial area of a contact device [12, 13].
The rigorous modelling leads to a system of differential–algebraic equations which has to be solved numerically. Special methods have been developed for the efficient treatment of such kind of problems, this will be treated in section 3.
In this paper only monodisperse aerosols are considered, i.e. the number concentration of wettable particles is treated as a constant input parameter. In a forthcoming paper, the modelling and simulation of polydisperse aerosols will be described, where population balances are used.

2 Modelling

2.1 Basic assumptions

Since the physical situation in an arbitrary gas–liquid contact device is far too complex for a detailed description, we have to set up a simplified model: The contact device is considered to be equivalent to two streams flowing side by side in contact with one another across some interfacial area A.

The competing heat and mass transfer processes between gas and liquid phase on the one side and between gas and dispersed phase on the other side have different time scales (i.e. seconds for the first and milliseconds for the latter process). Therefore, we have to find a common reference axis for the two processes. This is exactly the contact device's interfacial area A. Therefore, we can choose the interfacial area as independent coordinate. The fluid–dynamical complexities are entirely hidden in the device's mapping to its interfacial area. The connection between the actual device and its interfacial area can be taken from various publications [14, 15, 16, 17, 18, 19, 20, 21]. Introductory and elucidating examples can be found in the literature [22, 23]. Considering a plug flow in the contact device, a mapping of the spatial coordinate z to the interfacial area $A(z,t)$ according to

$$A(z,t) = A_\mathrm{c} \int_0^z a(z',t)\,\mathrm{d}z' \tag{2}$$

becomes possible. A_c and $a(z,t)$ are the local cross sectional area and the local specific interfacial area of the contact device, respectively. The specific interfacial area is defined as the derivative of the interfacial area of the entire contact device A with respect to the entire device's volume V:

$$a := \frac{\mathrm{d}A}{\mathrm{d}V} \quad . \tag{3}$$

Usually, A_c and a are supposed to be constant in space and time. Since A_c and and a are positive the mapping (2) between A and z is unique for every time t.
The general balance equation for an extensive physical quantity $F(\mathbf{r},t)$ can be written as [24, 25, 22]

$$\frac{\partial}{\partial t}\rho_F(z,t) + \frac{\partial}{\partial z} j_F = q_F(z,t) \tag{4}$$

where $\rho_F(z,t)$ is the local momentary volume density of F (in F units per volume), $j_F(z,t)$ is the local momentary flux of F (in F units per time and area), and $q_F(z,t)$ is the local momentary net production rate of F (in$F$ units per time and volume).
To express a given balance equation in the desired coordinates A and t we use

$$\frac{\partial A}{\partial z} = A_\mathrm{c}\, a(z,t) \tag{5}$$

which follows from equation (2) and get, using the uniqueness of $A(z,t)$,

$$\frac{\partial}{\partial z} j_F(z,t) = \frac{\partial A}{\partial z}\,\frac{\partial}{\partial A} j_F(A,t) = A_\mathrm{c}(z,t)\, a(z,t) \frac{\partial}{\partial A} j_F(A,t) \quad . \tag{6}$$

To transform the volume specific production rate q_F we have to take into account the volume V^{P} of the considered phase. This is given by

$$V^{\mathrm{P}}(z,t) = \int_0^z A_{\mathrm{c}}(z',t)\,\varepsilon^{\mathrm{P}}(z',t)\,\mathrm{d}z' \quad , \tag{7}$$

where $\varepsilon^{\mathrm{P}}(z,t)$ is the local momentary volume fraction of the phase P. Since $\varepsilon^{\mathrm{P}}(z,t)$ and A_{c} are positive there exists always an inverse function $z(V^{\mathrm{P}},t)$, which is – as an example – for constant ε^{P} simply given by

$$z = \frac{V^{\mathrm{P}}}{A_{\mathrm{c}}\,\varepsilon^{\mathrm{P}}} \quad . \tag{8}$$

In general, this inverse function is not given explicitely. Equations (2) and (7) yield for the interfacial area

$$A(V^{\mathrm{P}},t) = A_{\mathrm{c}} \int_0^{\frac{V^{\mathrm{P}}}{A_{\mathrm{c}}\,\varepsilon^{\mathrm{P}}}} a(z',t)\,\mathrm{d}z' \quad , \tag{9}$$

from which follows

$$\frac{\partial A(V^{\mathrm{P}},t)}{\partial V^{\mathrm{P}}} = \frac{a(V^{\mathrm{P}},t)}{\varepsilon^{\mathrm{P}}(V^{\mathrm{P}},t)} \quad . \tag{10}$$

This equation leads us finally to the expression for the volume specific production term in equation (4):

$$q_F(z,t) = \frac{a}{\varepsilon^{\mathrm{P}}}\,q_F(A,t) \quad . \tag{11}$$

Thus, the balance equation for an extensive physical quantity F within the phase P in coordinates A and t becomes

$$\frac{\varepsilon^P}{a}\frac{\partial}{\partial t}\rho_F(A,t) + \varepsilon^P A_{\mathrm{c}}\frac{\partial}{\partial A}j_F(A,t) = q_F(A,t) \quad . \tag{12}$$

Very often, other coordinates are more convenient, e.g. the overall number of transfer units $\mathrm{NTU}_i^{\mathrm{oG}}$ of a component i in absorption processes. This value is defined by

$$\mathrm{NTU}_i^{\mathrm{oG}}(z,t) = A_{\mathrm{c}} \int_0^z a(z',t)\frac{\beta_i^{\mathrm{oG}}(z',t)}{\dot{N}^{\mathrm{G}}(z',t)}\,\mathrm{d}z' \quad , \tag{13}$$

where $\beta_i^{\mathrm{oG}}(z,t)$ is the overall gas phase's momentary local mass transfer coefficient and $\dot{N}^{\mathrm{G}}(z',t)$ is the local momentary total mole flow of the gas phase.

A similar argumentation as above for equation (12) leads to the balance equation (4) in coordinates NTU_i and t:

$$\frac{\dot{N}^{\mathrm{G}}}{\beta_i^{\circ\mathrm{G}}} \frac{\varepsilon^P}{\mathrm{NTU}_i^{\circ\mathrm{G}}} \frac{\partial}{\partial t} \rho_F(\mathrm{NTU}_i, t) + \varepsilon^P A_{\mathrm{c}} \frac{\partial}{\partial \mathrm{NTU}_i} j_F(\mathrm{NTU}_i, t) = q_F(\mathrm{NTU}_i, t) \quad . \tag{14}$$

Equations (12) and (14) form the core of the model presented in this paper. For any generic quantity F we get the balance equations valid in our model from the classical conservation law simply by transformation with equation (12) or (14). This will be repeatedly shown in section 2.4 where the resulting system of PDEs is presented.
Usually, the density ρ_F and the flux j_F in the balance equations do not depend explicitly on A and t and therefore the transformation from equation (12) to equation (14) becomes to a simple multiplication of all time derivatives by the factor $\dot{N}^{\mathrm{G}}/\beta_i^{\circ\mathrm{G}}$ and expressing the production rate in terms of $q_F(\mathrm{NTU}_i)$ instead of $q_F(A)$.
For simplicity's sake the equations in the following text are only presented in coordinates A and t. Furthermore we assume constant values for ε^{P} for all phases.

2.2 Mass and Energy Transfer between Gas and Liquid Phase

Gradients of concentration and temperature lead to the transport of mass and energy within and among the phases. In our simplified, spatially one dimensional model there is only transport among the phases. Each phase itself is considered to be ideally mixed.
There are several different models describing these exchange processes in the literature. Convenient mass transfer equations in chemical engineering lead to a mole flux $\dot{n}_i$ of a component i in a K component system from the phase's interior to its border [22]

$$\dot{n}_i = j_i + y_i \sum_{k=1}^{K} \dot{n}_k = j_i + y_i \, \dot{n}_{\mathrm{t}} \quad . \tag{15}$$

In this equation

$$j_i = \beta_y^{\bullet} \, (y_i - y_i^{\star}) \tag{16}$$

is the diffusional mole flux caused by the difference between the mole–fraction y_i in the phase and the mole–fraction $y_i^{\star}$ at its border. $\beta_y^{\bullet}$ is the mass transfer coefficient in the presence of a non vanishing convectional mass flux[1].

[1] In German literature the mass transfer coefficient β_c is commonly referenced to molar concentrations and has the dimension m/s, while for our purposes the reference to mole

It can be calculated from the mass transfer coefficient without convection β_y by using film theory [26] or penetration theory [27]. Both options are implemented in **AerCoDe**.
The second term on the right hand sides of equation (15)

$$\dot{n}_{\mathrm{t}} = \sum_{k=1}^{K} \dot{n}_k \tag{17}$$

takes into account the effects of a mass transport perpendicularly to the interface which is caused by non–vanishing mass transfer rates $\dot{n}_{\mathrm{t}}$.
In analogy to equation (15) the energy flux from the phase's interior to its border can be written as

$$\dot{e} = \dot{q} + \sum_{k=1}^{K} \bar{H}_k \dot{n}_k \quad . \tag{18}$$

The second term on the right hand side represents the convectional energy transfer.
As in equation (16) the heat flux caused by the temperature difference between the phase's interior (T) and its border ($T^\star$) is given by

$$\dot{q} = \alpha^\bullet (T - T^\star) \quad . \tag{19}$$

Again, the heat transfer coefficient in the presence of non vanishing mass fluxes $\alpha^\bullet$ has to be calculated from the heat transfer coefficient without convection α. This can be done by applying either film or penetration theory [28].

2.3 Mass and Energy Transfer between Gas and Single Aerosol Droplets

To model the transfer processes between an aerosol and its surrounding gas phase, we have to consider the interactions between one droplet and the gas phase first. After that we assume that the entire aerosol behaves as an ensemble of independent single droplets.
We consider a single spherical droplet as shown in figure 1 in a surrounding gas phase of K components and one inert carrier gas. The droplet is assumed to be ideally mixed and floating along with the gas stream (no–slip assumption). The gas phase directly above the droplet's surface has mole fractions y_i^{D} which are considered to be equilibrium values to the given droplet composition x_i^{D},

fractions is more convenient. We use therefore β_y in the dimension of mol/s/m^2 . The relation between β_c and β_y is given by

$$\beta_y = \frac{\rho \beta_c}{M} \quad .$$

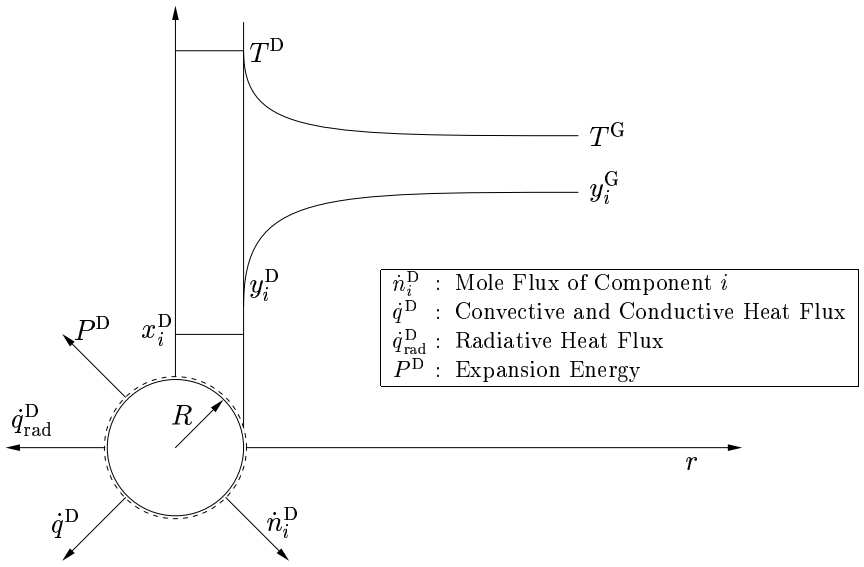

Figure 1: Concentration and temperature profiles in the surrounding of a single droplet

droplet temperature T^{D} and its radius R (Kelvin effect). The gas phase "far away" from the droplet has the temperature T^{G} and the composition y_i^{G}.
In the continuum regime where the droplet diameter is much bigger than the gas phase's mean free path, the solution of the generalized Stefan–Maxwell–Equations [29] yields for the mole flux of component i from a single droplet to the surrounding gas phase phase [30]

$$\dot{n}_i^{\mathrm{D}} = \frac{c^{\mathrm{G}} D_{i,\mathrm{gas}}}{R} \cdot \ln\left(\frac{1-y_i^{\mathrm{G}}}{1-y_i^{\mathrm{D}}}\right) \quad . \tag{20}$$

Approximating the thermal conductivity $\lambda(r)$ with the average values of the bulk gas phase (λ^{G}) and the value at the droplet's surface (λ^{D}) the heat flux from a single droplet to the gas phase can be written as

$$\dot{q}^{\mathrm{D}} = \frac{\lambda^{\mathrm{D}} + \lambda^{\mathrm{G}}}{2R} \cdot \left(T^{\mathrm{D}} - T^{\mathrm{G}}\right) \quad . \tag{21}$$

The radiative heat flux $\dot{q}^{\mathrm{D}}_{\mathrm{rad}}$ in figure 1 is neglected which is justified for droplets smaller than about 10 μm [31].
With the above equations, we finally obtain for the growth of a single droplet

$$\frac{Dn^{\mathrm{D}}}{Dt} = \frac{D(c^{\mathrm{D}} V^{\mathrm{D}})}{Dt} = -4\pi R^2 \sum_{k=1}^{K} \dot{n}_k^{\mathrm{D}} \quad . \tag{22}$$

With the droplet's volume $V^{\mathrm{D}} = 4/3\,\pi R^3$ this gives

$$\frac{DR}{Dt} = -\frac{1}{c^{\mathrm{D}}}\sum_{k=1}^{K}\dot{n}_k^{\mathrm{D}} - \frac{R}{3c^{\mathrm{D}}}\frac{Dc^{\mathrm{D}}}{Dt} \quad . \tag{23}$$

Similar derivations yield the balance for the droplet composition

$$\frac{Dx_i^{\mathrm{D}}}{Dt} = -\frac{3}{Rc^{\mathrm{D}}}\cdot\left[\dot{n}_i^{\mathrm{D}} - x_i^{\mathrm{D}}\sum_{k=1}^{K}\dot{n}_k^{\mathrm{D}}\right] \tag{24}$$

and the droplet temperature

$$\frac{DT^{\mathrm{D}}}{Dt} = -\frac{1}{\bar{C}_p^{\mathrm{D}}}\cdot\frac{3}{Rc^{\mathrm{D}}}\cdot\left[\sum_{k=1}^{K}\left(\bar{H}_k^{\mathrm{G}}(T^{\mathrm{D}}) - \bar{H}_k^{\mathrm{L}}(T^{\mathrm{D}})\right)\dot{n}_k^{\mathrm{D}} + \dot{q}^{\mathrm{D}}\right] \quad . \tag{25}$$

To follow the motion of the droplets in space and time, we have used in the above equations substantial derivatives

$$\frac{D}{Dt}\{...\} = \frac{\partial}{\partial t}\{...\} + v^{\mathrm{G}}\frac{\partial}{\partial z}\{...\} = \frac{\partial}{\partial t}\{...\} + A_c a\, v^{\mathrm{G}}\,\frac{\partial}{\partial A}\{...\} \quad , \tag{26}$$

see e.g. Bird et al. [22].

2.4 The Balance Equations

2.4.1 Mass and Energy Balance for the Gas–Liquid Interface

The gas–liquid interface is assumed to be in equilibrium with the both phases:

$$y_i^\star = \frac{p_i^\star}{p} = f(x_i^{\mathrm{L}}, T^\star) \quad . \tag{27}$$

Since we assume further no mass or energy accumulation in the gas–liquid interface, the balance equations for the interface interlink the fluxes between gas and liquid phase.
For the component mole balance, this simply results in

$$\dot{n}_i := \dot{n}_i^{\mathrm{G}} = \dot{n}_i^{\mathrm{L}} \quad . \tag{28}$$

The interface's energy balance can be used to determine the interfacial temperature $T^\star$:

$$\sum_{k=1}^{K}\left(\bar{H}_k^{\mathrm{G}}(T^{\mathrm{G}}) - \bar{H}_k^{\mathrm{L}}(T^{\mathrm{L}})\right)\cdot\dot{n}_k + \alpha^{\bullet\mathrm{G}}(T^{\mathrm{G}} - T^\star) - \alpha^{\bullet\mathrm{L}}(T^\star - T^{\mathrm{L}}) = 0 \quad . \tag{29}$$

2.4.2 Mass and Energy Balance for the Liquid Phase

To set up the mass balance equation for the liquid phase, we simply have to replace the generic quantity F in equation (12) by the total number of moles n^{L} in the liquid phase. The density ρ_F becomes the molar volume concentration c^{L} and the flux j_F becomes the product of c^{L} and the local momentary velocity v^{L} of the liquid phase. The net production rate q_F finally is replaced by the sum of all mole fluxes entering or leaving the liquid phase.
With the liquid phase's velocity

$$v^{\mathrm{L}} = \frac{\dot{N}^{\mathrm{L}}}{c^{\mathrm{L}} \varepsilon^{\mathrm{L}} A_{\mathrm{c}}} \tag{30}$$

and the molar volume concentration

$$c^{\mathrm{L}} = \frac{\rho^{\mathrm{L}}}{\bar{M}^{\mathrm{L}}} \tag{31}$$

the total mole balance of the liquid phase is given by

$$\frac{\varepsilon^{\mathrm{L}}}{a} \frac{\partial c^{\mathrm{L}}}{\partial t} = -\frac{\partial \dot{N}^{\mathrm{L}}}{\partial A} + \sum_{k=1}^{K} \dot{n}_k^{\mathrm{L}} \quad . \tag{32}$$

To derive the liquid phase's component mole balance for component i, F in equation (12) is replaced by the mole number $n_i^{\mathrm{L}} = x_i^{\mathrm{L}} \cdot n^{\mathrm{L}}$ of component i and the density is replaced by the product of molar volume concentration and the mole fraction x_i^{L}. The flux of component i is equal $x_i^{\mathrm{L}}\, c^{\mathrm{L}}\, v^{\mathrm{L}}$ (ignoring dispersive effects). The resulting mole balance of component i in the liquid phase is

$$\frac{\varepsilon^{\mathrm{L}} c^{\mathrm{L}}}{a} \frac{\partial x_i^{\mathrm{L}}}{\partial t} = -\dot{N}^{\mathrm{L}} \frac{\partial x_i^{\mathrm{L}}}{\partial A} + \beta_y^{\bullet}(y_i^{\mathrm{G}} - y_i^{\star}) + (y_i^{\mathrm{G}} - x_i^{\mathrm{L}}) \sum_{k=1}^{K} \dot{n}_k^{\mathrm{G}} \quad . \tag{33}$$

Replacing F in equation (12) by the inner energy $\bar{U}^{\mathrm{L}}$ of the liquid phase and using the definition of the enthalpy $H = U + pV$ yields the liquid phase's energy balance:

$$\frac{\varepsilon^{\mathrm{L}}}{a}\, c^{\mathrm{L}} \sum_{k=1}^{K} x_k^{\mathrm{L}} \frac{\partial \bar{H}_k^{\mathrm{L}}}{\partial t} = -\dot{N}^{\mathrm{L}} \sum_{k=1}^{K} x_k^{\mathrm{L}} \frac{\partial \bar{H}_k^{\mathrm{L}}}{\partial A} + \dot{q}^{\mathrm{L}} \quad . \tag{34}$$

Inserting the component mole balance (33), using the enthalpy's total differential

$$\mathrm{d}\bar{H} = \bar{C}_p\, \mathrm{d}T - \left[T \left(\frac{\partial \bar{V}}{\partial T} \right)_p - \bar{V} \right] \mathrm{d}p + \sum_{k=1}^{K} \frac{\partial \bar{H}}{\partial x_k}\, \mathrm{d}x_k \quad , \tag{35}$$

neglecting the thermal dilatation coefficient $(\frac{\partial \bar{V}_i^{\mathrm{L}}}{\partial T})_p$ and assuming $\partial p/\partial t = 0$ results with the heat flux (19) finally in the liquid phase's energy balance:

$$\frac{\varepsilon^{\mathrm{L}}}{a} c^{\mathrm{L}} \bar{C}_p^{\mathrm{L}} \frac{\partial T^{\mathrm{L}}}{\partial t} = -\dot{N}^{\mathrm{L}} \bar{C}_p^{\mathrm{L}} \frac{\partial T^{\mathrm{L}}}{\partial A} - \frac{\dot{N}^{\mathrm{L}}}{c^{\mathrm{L}}} \frac{\partial p}{\partial A} + \alpha^{\bullet \mathrm{L}} (T^{\star} - T^{\mathrm{L}}) \quad . \tag{36}$$

2.4.3 Mass and Energy Balance for the Gas Phase

The total mole balance for the gas phase is derived from equation (12) in the same way as the total mole balance for the liquid phase (32):

$$\frac{\varepsilon^{\mathrm{G}}}{a} \frac{\partial c^{\mathrm{G}}}{\partial t} = -\frac{\partial \dot{N}^{\mathrm{G}}}{\partial A} - \sum_{k=1}^{K} \dot{n}_k^{\mathrm{G}} + \sum_{k=1}^{K} \dot{n}_k^{\mathrm{A}} \quad . \tag{37}$$

Deriving the component mole balance for the gas phase considering axial dispersion effects (which are neglected in the liquid phase) works in principle the same way as for the liquid phase. The flow velocity v_i^{G} of component i now is given by the superposition of the average gas velocity v^{G} and the diffusional and dispersional velocities relative thereto. From equation (12) we get

$$\frac{\varepsilon^{\mathrm{G}}}{a} c^{\mathrm{G}} \frac{\partial y_i^{\mathrm{G}}}{\partial t} + \frac{\varepsilon^{\mathrm{G}}}{a} y_i \frac{\partial c^{\mathrm{G}}}{\partial t} = -y_i^{\mathrm{G}} \frac{\partial \dot{N}^{\mathrm{G}}}{\partial A} - \dot{N}^{\mathrm{G}} \frac{\partial y_i}{\partial A} - \dot{n}_i^{\mathrm{G}} + \dot{n}_i^{\mathrm{A}} - \varepsilon^{\mathrm{G}} A_{\mathrm{c}} \frac{\partial j_i}{\partial A} \quad . \tag{38}$$

Neglecting thermo–diffusional effects, we may write

$$j_i = -D_{i,\mathrm{mat}}\, c^{\mathrm{G}}\, \frac{\partial y_i^{\mathrm{G}}}{\partial z} \quad . \tag{39}$$

The material axial dispersion coefficient $D_{i,\mathrm{mat}}$ for laminar flows is given by [32]

$$D_{i,\mathrm{mat}} = D_{i,\mathrm{gas}} + \frac{(d\, v^{\mathrm{G}})^2}{192\, D_{i,\mathrm{gas}}} \quad . \tag{40}$$

For turbulent flows it is given by [33]

$$D_{\mathrm{mat}} = 5,05\, d\, v^{\mathrm{G}} \sqrt{\frac{\zeta}{8}} \quad . \tag{41}$$

In the above equations, d is a characteristic diameter of the device (e.g. the diameter of a single packing element) and ζ can be calculated using well known relations from fluid dynamics [34], e.g.

$$\zeta = \frac{l}{d} \frac{64}{\mathrm{Re}} \tag{42}$$

with a single packing element's length l and the Reynolds number Re.
Together with the total mole balance (37) this finally leads to the component mole balance for component i in the gas phase:

$$\begin{aligned}\frac{\varepsilon^{\mathrm{G}} c^{\mathrm{G}}}{a}\frac{\partial y_i^{\mathrm{G}}}{\partial t} = &- \dot{N}^{\mathrm{G}}\frac{\partial y_i^{\mathrm{G}}}{\partial A} - \beta_y^{\bullet}(y_i^{\mathrm{G}} - y_i^{\star}) + \dot{n}_i^{\mathrm{A}} - y_i^{\mathrm{G}}\sum_{k=1}^{K}\dot{n}_k^{\mathrm{A}} \\ &+ \varepsilon^{\mathrm{G}} A_{\mathrm{c}}^2 \frac{\partial}{\partial A}\left(a c^{\mathrm{G}} D_{i,\mathrm{mat}}\frac{\partial y_i^{\mathrm{G}}}{\partial A}\right) \quad .\end{aligned} \tag{43}$$

From equation (12) we get for the energy balance of the gas phase

$$\begin{aligned}\frac{\varepsilon^{\mathrm{G}}}{a}\frac{\partial(c^{\mathrm{G}}\bar{H}^{\mathrm{G}})}{\partial t} = &- \frac{\partial(\bar{H}^{\mathrm{G}}\dot{N}^{\mathrm{G}})}{\partial A} - \dot{q}^{\mathrm{G}} + \dot{q}^{\mathrm{A}} \\ &- \sum_{k=1}^{K}\bar{H}_k^{\mathrm{G}}\left(\dot{n}_k^{\mathrm{G}} - \dot{n}_k^{\mathrm{A}}\right) - \varepsilon^{\mathrm{G}} A_{\mathrm{c}}\frac{\partial j_q}{\partial A} \quad .\end{aligned} \tag{44}$$

Setting

$$j_q = -D_{\mathrm{th}} c^{\mathrm{G}} \bar{C}_p^{\mathrm{G}}\frac{\partial T^{\mathrm{G}}}{\partial z} + \sum_{k=1}^{K}\bar{H}_k^{\mathrm{G}} j_k \tag{45}$$

with the thermal axial dispersion coefficient for turbulent flows

$$D_{\mathrm{th}} = d\left(5.05 v^{\mathrm{G}}\sqrt{\frac{\zeta}{8}} + 2.515 v^{\mathrm{G}}\right) \tag{46}$$

and equal to the material one for laminar flows [35], we get finally the energy balance for the gas phase
With the enthalpy's total differential (35) this leads to the energy balance for the gas phase

$$\begin{aligned}\frac{\varepsilon^{\mathrm{G}}}{a} c^{\mathrm{G}} \bar{C}_p^{\mathrm{G}}\frac{\partial T^{\mathrm{G}}}{\partial t} = &- \bar{C}_p^{\mathrm{G}}\dot{N}^{\mathrm{G}}\frac{\partial T^{\mathrm{G}}}{\partial A} - \alpha^{\bullet\mathrm{G}}(T^{\mathrm{G}} - T^{\star}) + \dot{q}^{\mathrm{A}} \\ &+ \varepsilon^{\mathrm{G}} A_{\mathrm{c}}^2\frac{\partial}{\partial A}\left(a c^{\mathrm{G}}\bar{C}_p^{\mathrm{G}} D_{\mathrm{th}}\frac{\partial T^{\mathrm{G}}}{\partial A}\right) \quad .\end{aligned} \tag{47}$$

Here we have assumed again $\partial p/\partial t = 0$ and additionally $T(\partial \bar{V}_i/\partial T)_p - \bar{V}_i = 0$ which is exactly valid only for ideal gases.
Please note that in the above equations Taylor dispersion was used only as an example to demonstrate the capabilities of the presented model. Since we do not know if it is really applicable to gas–liquid contact devices and since we assume the effects to be negligible we usually ignore it in our simulations. But the model itself as well as the programme **AerCoDe** are able to handle this effect.

2.4.4 Mass and Energy Balance for the Aerosol

Since we do not yet consider effects like coagulation, deposition, or homogeneous nucleation the balance equation for the total number of droplets becomes quite simple: With the droplet number concentration c_{N} (in droplets per volume) we get for the "droplet flow" (in droplets per time)

$$\dot{N}^{\mathrm{D}} := \dot{N}^{\mathrm{G}} \frac{c_{\mathrm{N}}}{c^{\mathrm{G}}} \quad . \tag{48}$$

Even though we assume a constant number of wettable nuclei or droplets, the number concentration c_{N} is due to the temperature changes of the gas phase not constant in time and A. Only the droplet flow $\dot{N}^{\mathrm{D}}$ is constant. Neglecting dispersion effects leads in analogy to equations (32) and (37) to the balance equation for the droplet number equation:

$$\frac{\varepsilon^{\mathrm{G}}}{a} \frac{\partial c_{\mathrm{N}}}{\partial t} = - \frac{\partial}{\partial A} \left(\dot{N}^{\mathrm{G}} \frac{c_{\mathrm{N}}}{c^{\mathrm{G}}} \right) \quad . \tag{49}$$

With n^{D} being the total number of moles in one droplet, the total (liquid) mole flow carried along by the entire aerosol population is given by

$$\dot{N}^{\mathrm{A}} := n^{\mathrm{D}} \dot{N}^{\mathrm{D}} \quad . \tag{50}$$

From equation (12) we get immediately

$$\frac{\varepsilon^{\mathrm{G}}}{a} \frac{\partial}{\partial t} (n^{\mathrm{D}} c_{\mathrm{N}}) = - \frac{\partial \dot{N}^{\mathrm{A}}}{\partial A} - \sum_{k=1}^{K} \dot{n}_k^{\mathrm{A}} \quad . \tag{51}$$

With the balance for the number of droplets (49) and the definition of $\dot{N}^{\mathrm{A}}$ this yields

$$\frac{c_{\mathrm{N}} \varepsilon^{\mathrm{G}}}{a} \frac{\partial n^{\mathrm{D}}}{\partial t} = - \dot{N}^{\mathrm{D}} \frac{\partial n^{\mathrm{D}}}{\partial A} - \sum_{k=1}^{K} \dot{n}_k^{\mathrm{A}} \quad . \tag{52}$$

The source terms $\dot{n}_i^{\mathrm{A}}$ may be written as

$$\dot{n}_i^{\mathrm{A}}(z) = c_{\mathrm{N}} \, 4\pi R^2 \, \dot{n}_i^{\mathrm{D}} \tag{53}$$

or, using equation (11),

$$\dot{n}_i^{\mathrm{A}}(A) = \frac{\varepsilon^{\mathrm{G}} c_{\mathrm{N}}}{a} \, 4\pi R^2 \, \dot{n}_i^{\mathrm{D}} \quad . \tag{54}$$

With this equation and the relation $n^{\mathrm{D}} = c^{\mathrm{D}} \, 4\pi R^3/3$ one obtains from (52) again the mass balance for a single droplet, respectively the equation for the droplet radius, equation (23). Similar considerations hold for the aerosols component mole balance and its energy balance: For a monodisperse aerosol

the balance equations of single droplets and those of the entire droplet ensemble are, except for a scaling factor, completely equivalent.
Therefore we get the balances for the aerosol phase from the the corresponding equations for a single droplet simply by transforming the substantial derivatives in equations (23), (24) and (25) by means of (26). This gives the following equations for the droplet radius

$$\begin{aligned} \frac{\varepsilon^{\mathrm{G}}}{a}\,\frac{c^{\mathrm{G}}}{\dot{N}^{\mathrm{G}}}\left(\frac{\partial R}{\partial t}+\frac{R}{3\,c^{\mathrm{D}}}\,\frac{\partial c^{\mathrm{D}}}{\partial t}\right) &= -\left(\frac{\partial R}{\partial A}+\frac{R}{3\,c^{\mathrm{D}}}\,\frac{\partial c^{\mathrm{D}}}{\partial A}\right) \\ &\quad -\frac{\varepsilon^{\mathrm{G}}}{a}\,\frac{c^{\mathrm{G}}}{c^{\mathrm{G}}\,\dot{N}^{\mathrm{G}}}\cdot\sum_{k=1}^{K}\dot{n}_k^{\mathrm{D}} \quad , \end{aligned} \tag{55}$$

the droplet composition

$$\frac{\varepsilon^{\mathrm{G}}}{a}\,\frac{c^{\mathrm{G}}}{\dot{N}^{\mathrm{G}}}\,\frac{\partial x_i^{\mathrm{D}}}{\partial t} = -\,\frac{\partial x_i^{\mathrm{D}}}{\partial A}-\frac{\varepsilon^{\mathrm{G}}}{a}\,\frac{3\,c^{\mathrm{G}}}{R\,c^{\mathrm{D}}\,\dot{N}^{\mathrm{G}}}\cdot\left[\dot{n}_i^{\mathrm{D}}-x_i^{\mathrm{D}}\sum_{k=1}^{K}\dot{n}_k^{\mathrm{D}}\right] \quad , \tag{56}$$

and the droplet temperature

$$\begin{aligned} \frac{\varepsilon^{\mathrm{G}}}{a}\,c^{\mathrm{G}}\,\frac{\bar{C}_p^{\mathrm{D}}}{\dot{N}^{\mathrm{G}}}\,\frac{\partial T^{\mathrm{D}}}{\partial t} &= -\,\bar{C}_p^{\mathrm{D}}\,\frac{\partial T^{\mathrm{D}}}{\partial A} \\ &\quad -\frac{\varepsilon^{\mathrm{G}}}{a}\,\frac{3\,c^{\mathrm{G}}}{\dot{N}^{\mathrm{G}}\,R\,c^{\mathrm{D}}}\cdot\left[\sum_{k=1}^{K}\left(\bar{H}_k^{\mathrm{G}}-\bar{H}_k^{\mathrm{D}}\right)\,\dot{n}_k^{\mathrm{D}}+\dot{q}^{\mathrm{D}}\right] \quad . \end{aligned} \tag{57}$$

These above droplet equations complete our model.

3 Numerical Scheme

The whole system of balance equations consists of one–dimensional partial differential equations of convective type and of some pure algebraic equations. The space discretization of this system on an appropriate grid by the method of lines results in a very large system of differential–algebraic equations (DAEs).
We solved these systems using the extrapolated linearly–implicit Euler method with an adaptive control of step size and order, the LIMEX–code [36]. This method enables an effective integration even of large sparse systems using iterative solvers and a flexible incomplete factorization of the linear systems. Furthermore the code detects inconsistent initial values of a DAE system and can compute consistent ones.

4 Application: Simulation of a Multi Stage Absorption Process

As a demonstration of the capabilities of the above presented model and its implementation in **AerCoDe**, we present the simulation results of a two stage gas cleaning process. A hot flue gas is first quenched in an adiabatic co–current packed column and then cleaned in a counter current packed column (see figure 2).
For this simulation we use the following assumptions and models:

- The number of wettable condensation nuclei c_N and their critical saturation $\mathbf{S}_{crit}$ are given input parameters. Even though there are theories to calculate these values from contact angles and surface tensions (e.g. [37]) missing data make theoretical predictions concerning these parameters unreliable. So we use experimentally determined values [6, 38, 39] or treat c_N and $\mathbf{S}_{crit}$ as input parameters. The critical saturation was set to unity for all simulations.

- Physical properties (surface tension, enthalpies, densities etc.) and phase equilibria of the system HCl/H_2O/Air are taken from the literature [40, 41].

- The growth of the droplets is calculated according to Kulmala et al. [42].

- The specific interfacial area, HTU and NTU values, heat and mass transfer coefficients for the packing are calculated according to Billet [43, 44].

The composition and flow rates entering the first stage are given in table 1. In Gretscher's experiments, the number concentration of foreign nuclei available for the heterogeneous nucleation process is typically $1.0 \cdot 10^5\,\mathrm{cm}^{-3}$. The inlet pressure is 98500 Pa and the first stage's pressure drop is 700 Pa. The washing liquid is pure water. The packing consists of Ceramic–Hiflow–Rings Type 20–4 in the upper (hot) third of the quench and of PP–Hiflow–Rings Type 25–7 in the lower (cool) part.
Table 2 shows the simulation results for the first stage without aerosol formation and with an aerosol number concentration of $1.0 \cdot 10^5\,\mathrm{cm}^{-3}$.
Figure 3 shows the calculated saturation profile for different number concentrations of nuclei. Until the saturation reaches unity (at an NTU value of 4.3) the plotted profiles do not differ. But due to the onset of heterogeneous nucleation and droplet growth the different number concentrations take effect beyond this point. The more nuclei (and thus the more droplets) we have in the gas phase the faster the supersaturation is decreasing because of the droplet growth. But even without droplets, the saturation tends back to unity because of the system's urge to equilibrium at infinite values of the

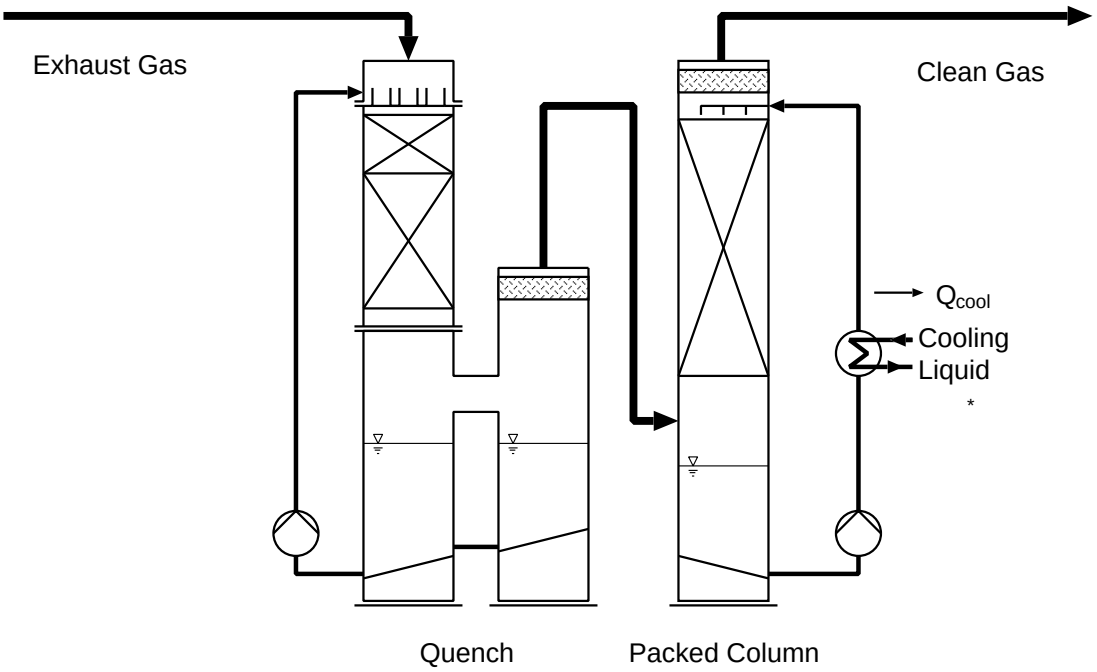

Figure 2: Experimental setup

Table 1: Input data for the adiabatic quench cooler

Input data of the first stage	Gas Phase	Washing Liquid
total flow rate [kg/h]	257.33	2988.00
inert gas flow rate [kg/h]	252.00	
H_2O flow rate [kg/h]	5.04	2988.00
HCl flow rate [kg/h]	0.29	0.00
temperature [^{o}C]	200.0	
H_2O load [kg H_2O / kg inert gas]	0.02	1.00
HCl load [kg HCl / kg inert gas]	0.0011	0.00

interfacial aerea A. Figure 4 shows the calculated droplet diameters in the quench for different number concentrations. Obviously fewer droplets lead to bigger droplet diameters.

This can be explained by the fact that more droplets provide more interfacial area between gas phase and aerosol as shown in figure 5. This leads to higher mass flows from the gas phase to the aerosol population (see figure 6) and consequently to a higher total mass of the aerosol population in the first stage's outlet.

The fast decrease of the saturation at high number concentrations of droplets slows down the droplet growth. Consequently, the entire mass flow to a single droplet is smaller at higher number concentrations as shown in figure 7. Thus, although more droplets withdraw more matter from the gas phase, higher number concentrations lead to smaller droplets.

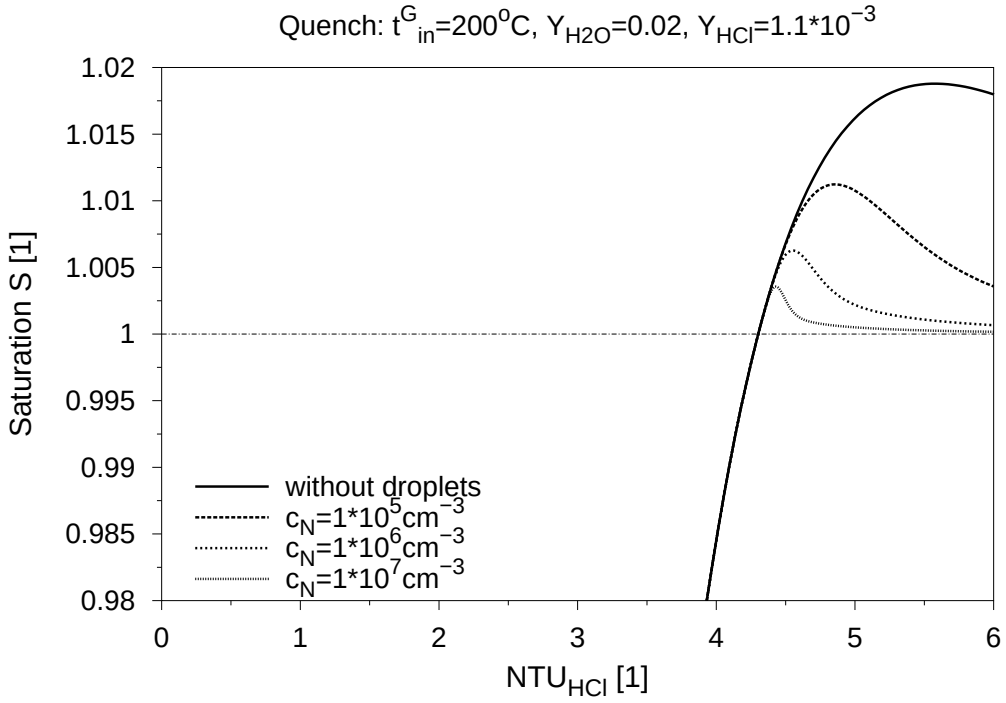

Figure 3: Calculated saturation profiles in the quench for different number concentrations of nucleation kernels

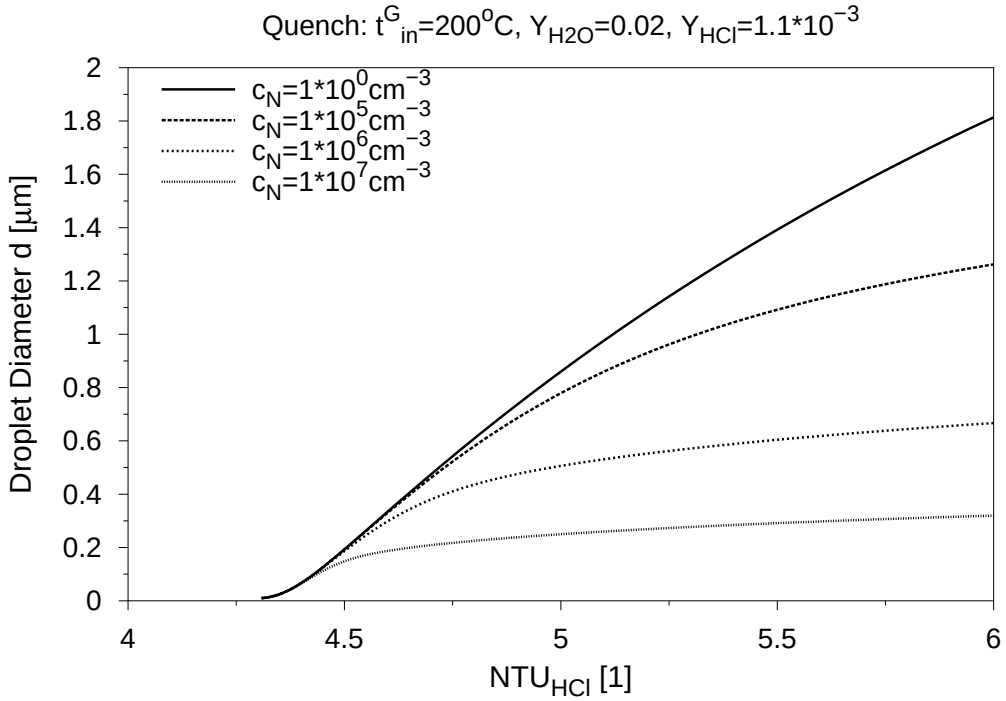

Figure 4: Calculated droplet diameters in the quench for different number concentrations of nucleation kernels

Table 2: Simulation results for the adiabatic quench cooler without aerosol formation (differing results with $c_N = 1 \cdot 10^5\,cm^{-3}$ are given in parenthesis)

Output data of the first stage	Gas Phase	Washing Liquid
total flow rate [kg/h]	273.78	2971.27 (2971.25)
inert gas flow rate [kg/h]	252.00	
H_2O flow rate [kg/h]	21.78	2971.27 (2971.25)
HCl flow rate [kg/h]	$7.6 \cdot 10^{-4}$ ($4.4 \cdot 10^{-4}$)	0.29
temperature [^{o}C]	50.15 (50.29)	49.97
H_2O load [kg H_2O / kg inert gas]	0.086	0.999
HCl load [kg HCl / kg inert gas]	$3.01 \cdot 10^{-6}$ ($1.763 \cdot 10^{-6}$)	$9.7 \cdot 10^{-5}$

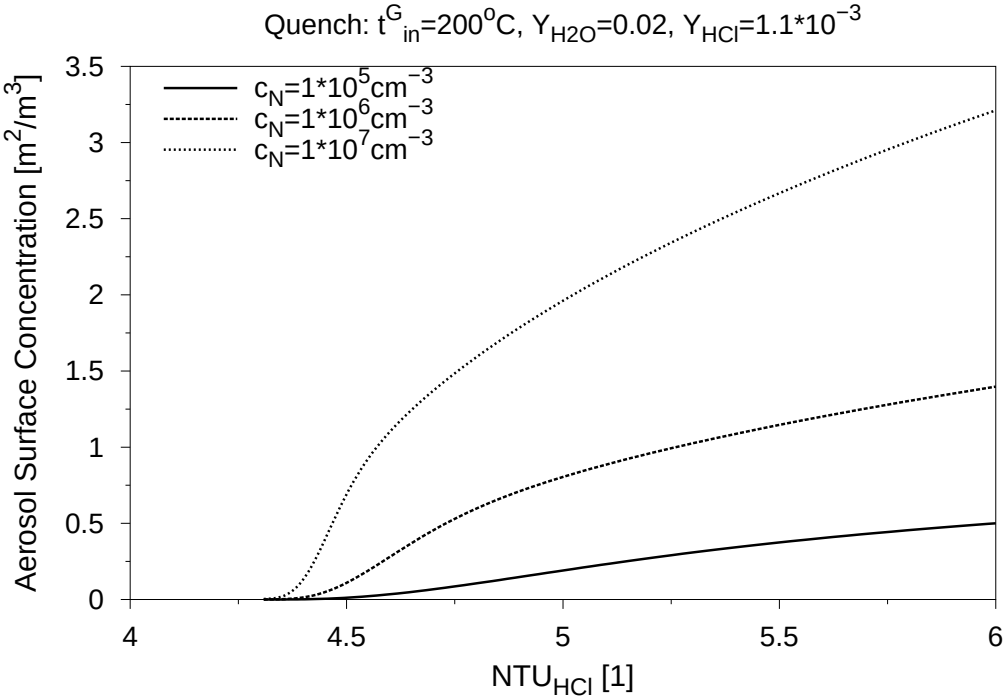

Figure 5: Surface of the entire aerosol population for different number concentrations of nucleation kernels

The simulation results for the quench simulation with $c_N = 1 \cdot 10^5\,cm^{-3}$ agree well with the experimental data published by Gretscher [39, 6]. He measures with the given process conditions a droplet diameter of 1.2 micrometers at the first stages' outlet (NTU $\approx$ 6). More comparisons between experimental and calculated data can be found in his thesis [39].
The simulation results of the first stage were used as input for the simulation of the second stage (non–adiabatic, counter current column). The cooling rate $\dot{Q}_{cool}$ is 3.0 kW, which results in an inlet temperature of the recycled washing liquid of 30°C. The packing consists of PP–Hiflow–Rings Type 25–7. The pressure drop is 500 Pa.

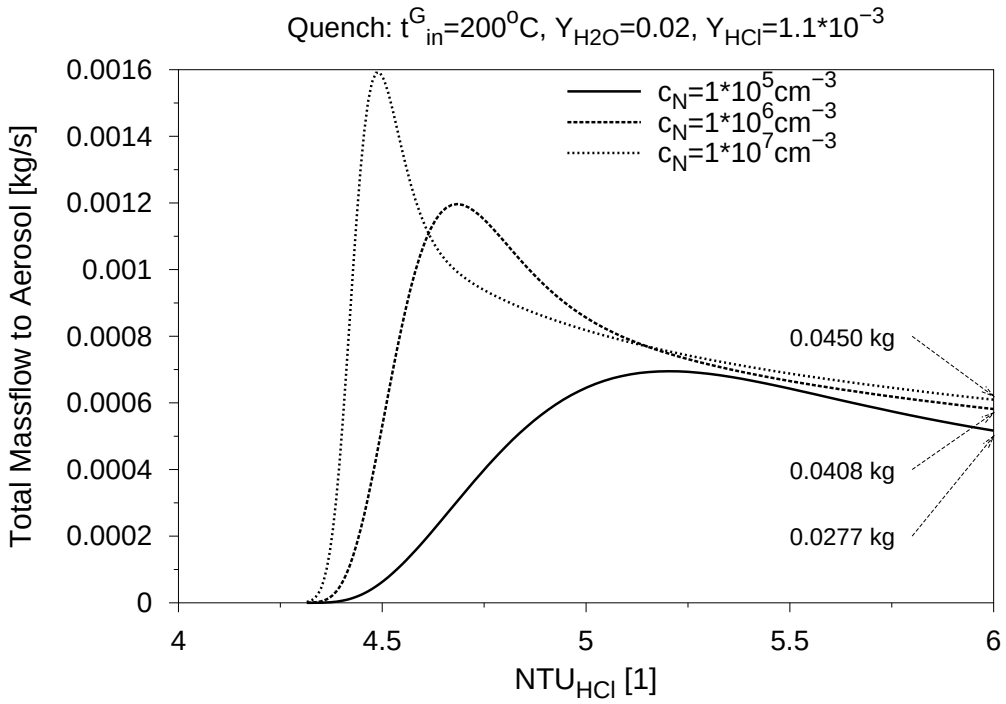

Figure 6: Massflow to the entire aerosol population for different number concentrations of nucleation kernels and resulting total aerosol mass in the outlet

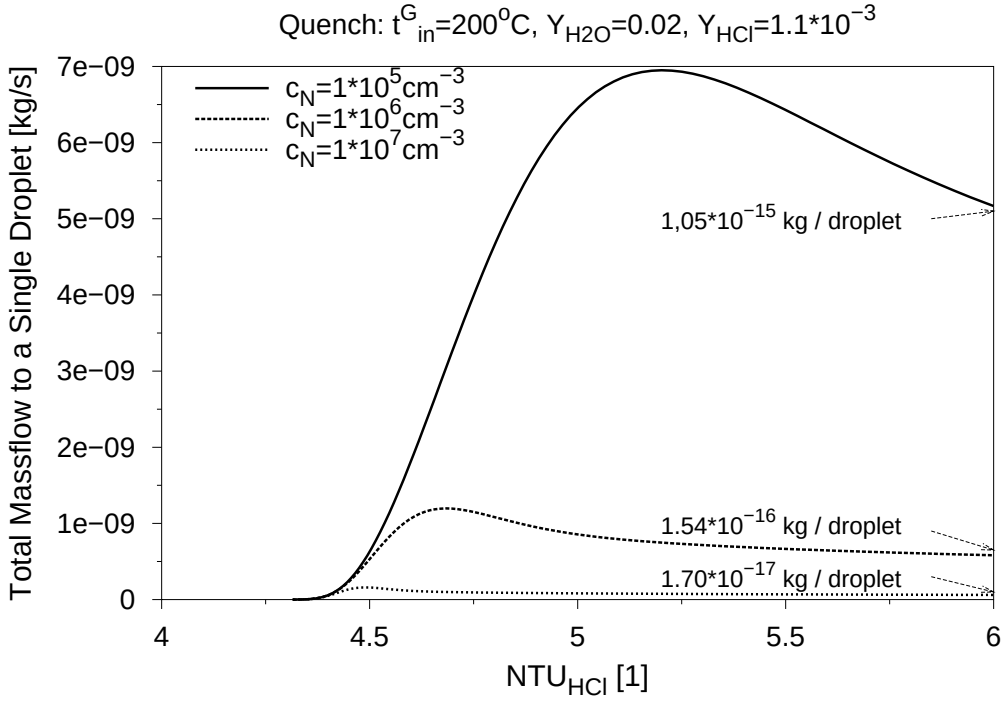

Figure 7: Massflow to a single droplet for different number concentrations of nucleation kernels and resulting droplet mass in the outlet

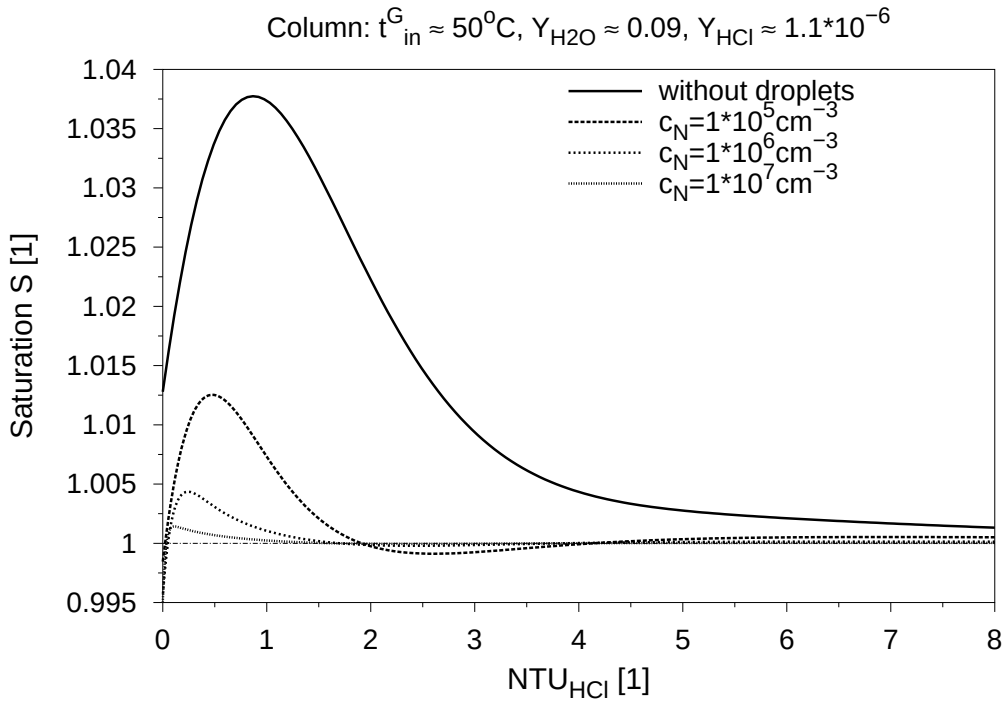

Figure 8: Calculated saturation profiles in the column for different number concentrations of nucleation kernels

The saturation profiles for the above number concentrations are shown in figure 8. Evidently, the gas phase reaches equilibrium ($\mathbf{S} = 1$) at the end of the column for all number concentrations. The more droplets in the gas the faster the supersaturation of the gas phase decreases since the droplets withdraw water and hydrogen chloride from the gas phase. But even without droplets, the gas phase reaches equilibrium at the end of the packed column if the NTU value (and therefore the interfacial area) is high enough.
In figure 9 the growth of the droplets entering the second stage is shown. Again, lesser droplets grow to bigger radii. The same considerations concerning the droplet growth in the first stage hold here.
The totally emitted pollutant concentration is the sum of the gas phase's pollutant concentration and the droplets' contribution thereto. Figure 10 shows the totally emitted amount of the pollutant (hydrogen chloride in this case). Even though the droplets at the higher number concentration are the smaller, their impact on the gas cleaning efficiency is worse. Even worse is the fact, that smaller droplets are harder to withdraw from the gas stream leaving the contact device than larger ones.

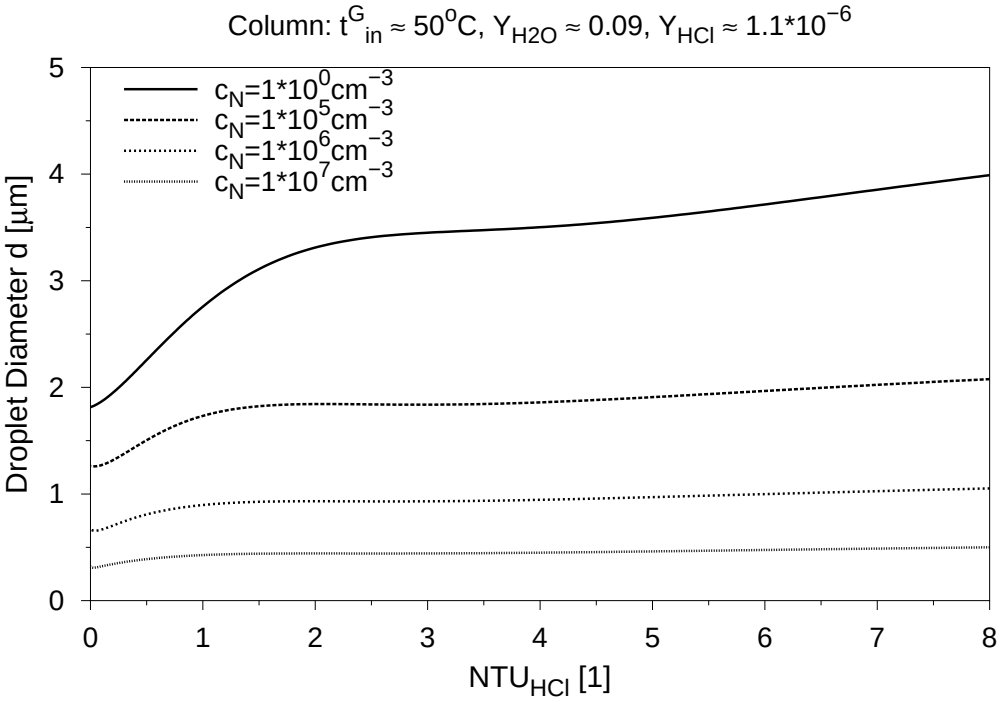

Figure 9: Calculated droplet diameters in the column for different number concentrations of nucleation kernels

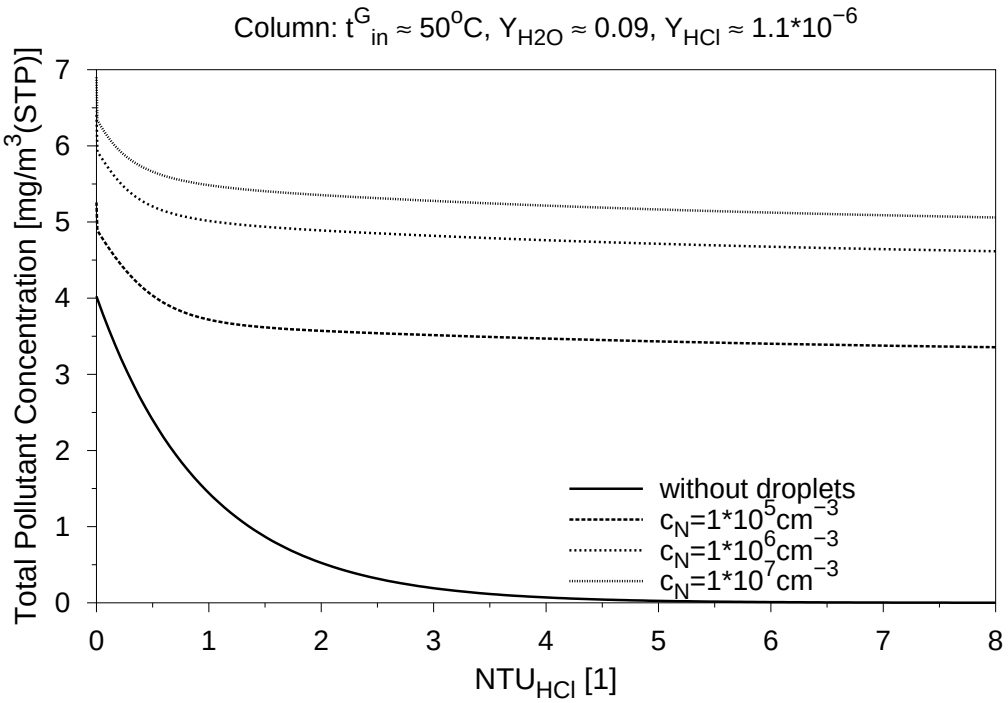

Figure 10: Calculated total pollutant concentration in the column for different number concentrations of nucleation kernels

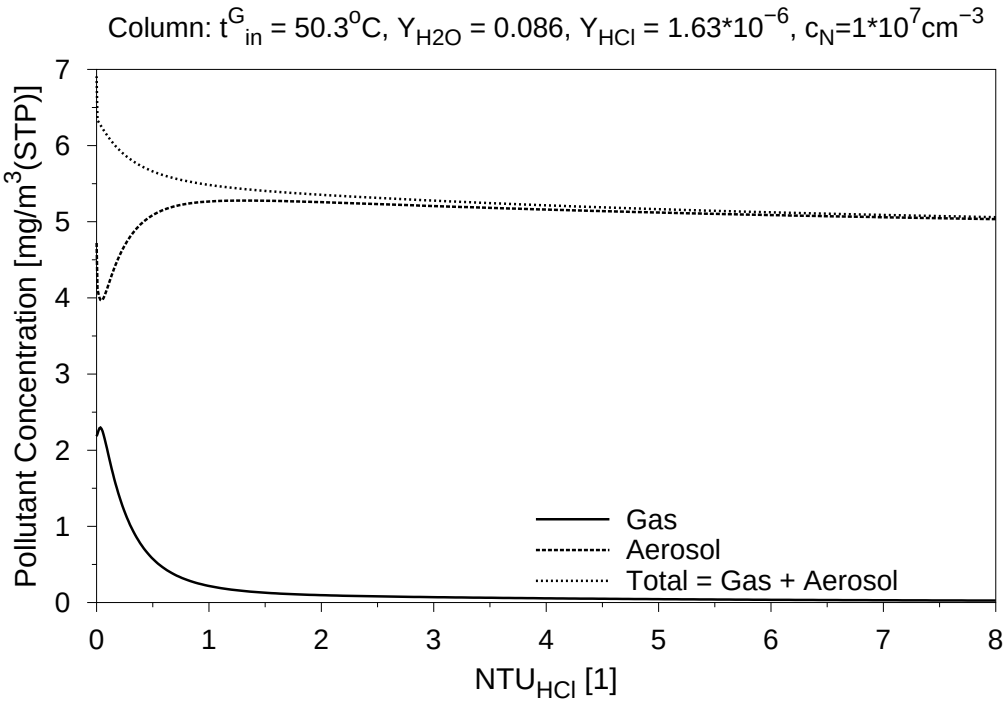

Figure 11: Calculated pollutant concentration in the column for $c_{\mathrm{N}} = 1.0 \cdot 10^6\,\mathrm{cm}^{-3}$.

In figure 11 this worst case (highest number concentration and smallest droplets) is demonstrated separately. The gas phase itself gets cleaned well (less than 0.03 mg HCl per standard cubic meter inert gas) but the HCl carried downstream by the droplets leads to a total pollutant concentration in the column's outlet of about 5 mg HCl per standard cubic meter inert gas. Commercial plant simulation tools are usually not able to handle aerosol formation and therefore predict lower pollutant concentrations (i.e. the lower curves in figures 10 and 11) than our tool **AerCoDe**.

5 Conclusions

The presented model of aerosol formation in gas–liquid contact devices and its implementation are powerful instruments for gaining insight in the formation and behaviour of aerosol droplets in technical plants. **AerCoDe** is a useful utility for making parameter studies on aerosol behaviour. Especially the latter is of great practical importance for minimising (or sometimes even avoiding) aerosol problems in industrial processes.
Currently further improvements as population balancing, refined numerical methods, and an extension of the implemented technical and physical systems are done.

Acknowledgements

We wish to thank the Deutsche Forschungsgemeinschaft for the financial support of this project.

Nomenclature

Symbol	Meaning	Unit
A	interfacial area	m^2
A_c	cross sectional area	m^2
a	specific interfacial area	m^2 / m^3
$\bar{C}_p$	molar heat capicity at constant pressure	J / mol / K
$\bar{C}_{pi}$	partial molar heat capicity at constant pressure of component i	J / mol / K
c	molar volume concentration	mol / m^3
c_N	particle number concentration	particles / m^3
$D_{i,gas}$	diffusion coefficient of component i in gas phase	m^2 / s
$D_{mat i}$	material axial dispersion coefficient of component i	m^2 / s
D_{th}	thermal axial dispersion coefficient of component i	m^2 / s
d	diameter	m
$\dot{e}$	energy flux	J / m^2 / s = W / m^2
F	generic extensive physical quantity	F units
$\bar{H}$	molar enthalpy of a mixture	J / mol
$\bar{H}_i$	partial molar enthalpy of component i	J / mol
$\mathbf{j}_F$, j_F	flux of generic physical quantity F	F units / m^2 / s
K	number of material components	1
l	length	m
M	molar mass	kg / mol
$\bar{M}$	a mixture's average molar mass	kg / mol
$\dot{N}$	mole flow	mol / s
$\dot{n}$	mole flux	mol / s / m^2
n	mole number	mol
NTU_i	number of transfer units of component i, see eq. (13) for definition	1
p	total pressure	Pa
p_s	total equilibrium pressure at dew point	Pa
$\dot{q}$	heat flux	J / m^2 / s = W / m^2
q_F	net production rate of generic physical quantity F	F units / m^3 / s
R	droplet radius	m
$\mathbf{r}$	vector in physical space	m
$\mathbf{S}$	saturation ratio	1
$\mathbf{S}_{crit}$	critical saturation ratio	1
T	temperature	K

Symbol	Meaning	Unit
t	time	s
V	volume	m^3
$\bar{V}$	molar volume	m^3 / mol
$\bar{V}_i$	partial molar volume of component i	m^3 / mol
x_i	liquid mole fraction of component i	1
y_i	gas mole fraction of component i	1
z	spatial coordinate	m
α	heat transfer coefficient without convection	W / K / m^2
$\alpha^\bullet$	heat transfer coefficient with convection	W / K / m^2
β_c	mass transfer coefficient without convection with respect to molar concentration	m / s
$\beta_c^\bullet$	mass transfer coefficient with convection with respect to molar concentration	m / s
β_y	mass transfer coefficient without convection with respect to mole fraction	mol / m^2 / s
$\beta_y^\bullet$	mass transfer coefficient with convection with respect to mole fraction	mol / m^2 / s
λ	thermal conductivity	J / s / m / K
ε	volume fraction	1
ρ_F	volume density of generic physical quantity F	F units / m^3

Superscript	Meaning
A	aerosol
D	single droplet
G	gas phase
L	liquid phase
P	arbitrary phase
$\star$	interface, equilibrium

Subscript	Meaning
i, j, k	component and summation indices
mat	material
th	thermal
crit	critical

References

[1] K. Schaber, Aerosolbildung durch spontane Phasenübergänge bei Absorptions– und Kondensationsprozessen, Chemie Ingenieur Technik 67 (11) (1990) 1443–1452.

[2] S. Kaufmann, Y. Loretz, K. Hilfiker, Prevention of Fog in a Condenser by Cimultaneous Heating and Cooling, Heat and Mass Transfer 32 (1997) 403–410.

[3] M. Ulbrich, S. Meckl, Theorie und Praxis bei Rauchgaswäschen, Chemie Ingenieur Technik 70 (3) (1998) 246–253.

[4] W. C. Hinds, Aerosol Technology – Properties, Behaviour, and Measurement of Airborne Particles, John Wiley & Sons, New York, 1982.

[5] S. Haep, M. Luckas, K.-G. Schmidt, Binary Heterogeneous Nucleation in Gas Cleaning Absorption Processes: Estimating the Critical Saturation rate of H_2O–Vapour and acid concentration inside the formed aerosol in a H_2O/HCl-Acid system, Journal of Aerosol Science 29, Suppl. 1 (1998) 133–S134.

[6] H. Gretscher, K. Schaber, Aerosol Formation by Heterogeneous Nucleation in Wet Scrubbing Processes, Chemical Engineering and Processing 38 (1999) 541–548.

[7] K. Schaber, Aerosol Formation in Absorption Processes, Chemical Engineering Science 50 (8) (1995) 1347–1360.

[8] A. P. Colburn, A. C. Edison, Prevention of Fog in Cooler–Condensers, Industrial Engineering Chemistry 33 (1941) 457–458.

[9] A. G. Amelin, Theory of Fog Condensation, Israel Program for Scientific Translations .

[10] D. E. Steinmeyer, Fog Formation in Partial Condensers, Chemical Engineering Progress 68 (7) (1972) 64–68.

[11] B. Sachweh, K. Hölemann, M. Ulbrich, W.-S. Weißker, Aerosolbildung in chemischen Prozessen: Innovative Problemlösungen durch intelligente Verknüpfung von Experiment und Simulation, Chemie Ingenieur Technik 71 (9) (1999) 946–947.

[12] J. Körber, K. Schaber, Modelling of Heat and Mass Transfer with Fog Formation, in: Proceedings of the 10th International Heat Transfer Conference, Brighton, 1994.

[13] J. Körber, K. Schaber, R. Ehrig, P. Deuflhard, Modelling and Simulation of Aerosol Formation in Absorption Processes, Journal of Aerosol Science 29, Suppl. 1 (1998) 579–580.

[14] R. Billet, J. Marckowiak, Liquid Phase Mass Transfer in Absorbtion Packed Columns, Chemical Engineering Communications 3 (1979) 1–14.

[15] R. Billet, J. Marckowiak, Hiflow-Ring, ein Hochleistungsfüllkörper für Gas–Flüssig–Systeme, Sonderdruck aus Chemie–Technik 13 (12) (1984) 37–36.

[16] J. L. Bravo, J. A. Rocha, J. R. Fair, Mass Transfer in Gauze Packings, Hydrocarbon Processing 91.

[17] J. L. Bravo, J. A. Rocha, J. Fair, A Comprehensive Model for the Performance of Columns Containing Structured Packings, ICHEME Symposium Series 128 (1992) A439.

[18] H. Chan, J. R. Fair, Prediction of Point Efficiencies in Sieve Trays: 1. Binary Systems, 2. Multicomponent Systems, Ind. Eng. Chem. Process Des. Dev. 23 (1984) 814.

[19] J. A. Grester, A. B. Hill, N. N. Hochgraf, D. Robinson, Tray Efficiencies in Distillation Columns, AIChe Report .

[20] K. Onda, H. Takeuchi, Y. Okumoto, Mass Transfer Coefficients between Gas and Liquid Phases in Packed Columns, Journal of Chemical Engineering Japan 1 (1968) 56.

[21] R. D. Scheffe, R. H. Weiland, Mass Transfer Characteristics of Valve Trays, Industrial & Engineering Chemisty Research 26 (1987) 228–236.

[22] R. B. Bird, W. E. Stewart, E. N. Lightfoot, Transport Phenomena, John Wiley & Sons, New York, 1960.

[23] H. D. Baehr, K. Stephan, Wärme– und Stoffübertragung, Springer–Verlag, 1994.

[24] W. M. Deen, Analysis of Transport Phenomena, Oxford University Press, New York ; Oxford, 1998.

[25] J. Warnatz, U. Maas, Technische Verbrennung, Springer–Verlag, Berlin, 1993.

[26] W. K. Lewis, W. G. Whitman, Principles of Gas Absorption, Industrial and Engineering Chemistry 116 (1924) 1215–1220.

[27] R. Higbie, The Rate of Absorption of a Pure Gas into a still Liquid During Short Periods of Exposure, Transactions of the American Institution of Chemical Engineers 31 (1935) 36–38.

[28] R. Krishna, G. L. Standart, Mass and energy transfer in multicomponent systems, Chemical Engineering Communications 3 (1979) 201–289.

[29] R. Taylor, Coupled heat and mass transfer in multicomponent systems: Solution of the maxwell–stefan equations, Letters in Heat and Mass Transfer 8 (1981) 405–416.

[30] J. C. Barret, C. F. Clement, Growth Rates for Liquid Droplets, Journal of Aerosol Science 19 (2) (1988) 223–242.

[31] O. Preining, P. E. Wagner, F. G. Pohl, W. Szymanski, Heterogeneous Nucleation and Droplet Growth, in: Abstracts of the Annual Conference of the Association for Aerosol Research, Vol. 20 of European Aerosol Conference: Proceedings of the European Aerosol Conference, 1989.

[32] G. Taylor, The Dispersion of Soluble Matter in Solvent Flowing Slowly through a Tube, Proceedings of the Royal Society A 219 (1953) 186–203.

[33] G. Taylor, The Dispersion of Matter in Turbulent Flow through a Pipe, Proceedings of the Royal Society A 223 (1954) 446–468.

[34] J. H. Spurk, Strömungslehre – Einführung in die Theorie der Strömungen, Springer–Verlag, 1989, 2., überarb. u. erw. Aufl.

[35] L. V. Beckman, V. J. Law, R. V. Bailey, D. U. Rosenberg, Axial Dispersion for Turbulent Flow with Large Radial Heat Flux, AIChE Journal 36 (1990) 598–604.

[36] P. Deuflhard, J. Lang, U. Nowak, Adaptive Algorithms in Dynamical Process Simulation, 8th Conference of the European Consortium for Mathematics in Industry, Kaiserslautern .

[37] N. Fletcher, Size Effect in Heterogeneous Nucleation, Journal of Chemical Physics 29 (1958) 572–576.

[38] H. Gretscher, K. Schaber, Basic Aerosol Science: Nucleation - Determination of active condensation nuclei for the aerosol formation in absorption and condensation processes, Journal of Aerosol Science 30 (1) (1999) 29–34.

[39] H. Gretscher, Entstehung von Aerosolen durch heterogene Keimbildung bei der Absorption und Kondensation, no. 650 in Fortschritt–Berichte VDI, Reihe 3, VDI Verlag, 2000.

[40] S. Brandani, V. Brandani, G. Di Giacomo, Vapor–Liquid Equilibrium Calculation of the System Water–hydrogen chloride, Fluid Phase Equilibria 92 (1994) 67–74.

[41] J. Liu, J. Koerber, K. Schaber, Berechnung des Dampf–Flüssigkeits-gewichts von wässriger Salzsäure, Wissenschaftlicher Abschlussbericht, 31. Internat. Seminar Universität Karslruhe .

[42] M. Kulmala, A. Laaksonen, J. Jokiniemi, Numerical Simulation of Binary Nucleation of Hydrogen Iodide and Water Vapours, Journal of Aerosol Science 22 (1991) 149–157.

[43] R. Billet, Fluiddynamik und Stoffübertragung bei der Gegenstrom–Absorption in Füllkörperkolonnen, Chemie–Umwelt–Technik (1991) 75–81.

[44] R. Billet, Stand der Entwicklung von Füllkörpern und Packungen und ihre optimale geometrische Oberfläche, Chemie Ingenieur Technik 64 (5) (1992) 401–410.